Electrical transport and photovoltaic effects of core–shell CuO/C_{60} nanowire heterostructure

2009 Nanotechnology 20 065203

(http://iopscience.iop.org/0957-4484/20/6/065203)

Nanotechnology **20** (2009) 065203 (8pp) doi:10.1088/0957-4484/20/6/065203

Electrical transport and photovoltaic effects of core–shell CuO/C_{60} nanowire heterostructure

Qiaoliang Bao[1,2], Chang Ming Li[1,6], Lei Liao[3], Hongbin Yang[1], Wei Wang[1], Chang Ke[4], Qunliang Song[1], Haifeng Bao[1], Ting Yu[3], Kian Ping Loh[2] and Jun Guo[5]

[1] School of Chemical and Biomedical Engineering, Nanyang Technological University, 70 Nanyang Drive, Singapore 637457, Singapore
[2] Department of Chemistry, National University of Singapore, 3 Science Drive 3, Singapore 117543, Singapore
[3] Division of Physics and Applied Physics, School of Physical and Mathematical Sciences, Nanyang Technological University, Singapore 637616, Singapore
[4] Microelectronics Centre, School of Electrical and Electronic Engineering, Nanyang Technological University, Nanyang Avenue, Singapore 639798, Singapore
[5] School of Materials Science and Engineering, Nanyang Technological University, Nanyang Avenue, Singapore 639798, Singapore

E-mail: ecmli@ntu.edu.sg

Received 29 September 2008, in final form 23 November 2008
Published 14 January 2009
Online at stacks.iop.org/Nano/20/065203

Abstract
An organic/inorganic hybrid heterostructure consisting of p-type CuO nanowire core and n-type C_{60} shell was fabricated and its electrical transport properties were studied for the first time. It was found that the devices with contacts on shell–shell show an ohmic behavior but the devices with contacts on core–shell forms a single p–n junction and display a rectifying behavior. Logarithmic current–voltage curves at various temperatures show that the tunneling transport plays a critical role in the electrical transport. Photovoltaic effects were observed in the core–shell contacted CuO/C_{60} junctions under illumination. This work demonstrates that an inorganic/organic coaxial nanowire can provide potential in nanoelectronic devices and could further stack high density hybrid nanowires array as a renewable power source.

(Some figures in this article are in colour only in the electronic version)

1. Introduction

Hybrid inorganic–organic cells are one of the promising excitonic solar cells for economic and large-scale solar energy conversion because the advantage resulting from two types of materials with low cost and easy preparation from the organic material and high electron mobility from the inorganic semiconductors [1–3]. In the last decade, researchers fabricated inorganic–organic heterojunctions by depositing organic molecules (C_{60}, C_{70}) on inorganic bulk materials (Si [4, 5], GaN [6, 7]) to form a plane interface. However, the efficiency of photovoltaic (PV) devices based on such a structure was very poor due to the limitation of diffusion length and light absorption coefficient. Since the breakthrough in dye-sensitized photoelectrochemical cells on nanocrystalline TiO_2 [1], the research activities on inorganic–organic devices by using several inorganic semiconductors with various nanostructures have increased enormously. Semiconductor nanostructures such as CdTe nanorods [8, 9], CdSe nanocrystals [10, 11] and nanoparticles of ZnO [12–14], PbS [15] and HgTe [16] were blended with conjugated polymers to yield a large number of nanocrystal–polymer interfaces for improved power conversion efficiency in this type of hybrid solar cell. To date, a random mixture of inorganic and organic materials has given the highest efficiency. However, it suffers from high resistance

[6] Author to whom any correspondence should be addressed.

which causes inefficient electron transport in relatively long collection length and from complicated interfaces that prohibit a detailed understanding of different aspects regarding electronic and structural properties. These greatly limit its commercialization in solar cells. Therefore, there is a great need to deeply understand the fundamentals of the hybrid organic/inorganic PV cell and then construct a new architecture of such types of device for high performance solar energy conversion.

Coaxial core–shell structured nanowires have been theoretically demonstrated to enhance carrier collection and overall efficiency with respect to single-crystal bulk semiconductors of the same material because its high aspect ratio allows us to use a sufficient thickness for good optical absorption while simultaneously providing short collection lengths for excited carriers in a direction normal to the light absorption [17, 18]. The recent progress in experiments also shows that the core–shell Si p–n junction solar cells could be very attractive for a nanoelectronic power source [19] and low cost solar cell [20]. However, hybrid inorganic–organic core–shell nanowire heterostructures have rarely been studied as nanoelectronic and PV devices. In this work, a simple and efficient method was developed to fabricate a core–shell CuO/C_{60} nanowire heterostructure and its new type of solar cell. CuO is an important p-type semiconductor with a bandgap of about 1.35 eV [21, 22] and C_{60} is an efficient n-type electron acceptor [23, 24] with a bandgap of about 1.5–2.0 eV [25]. By selecting these two materials to construct a heterojunction, we can not only study the fundamentals of an organic/inorganic heterojunction, but also can demonstrate a new type of nanoelectronic and PV device.

2. Experimental details

The CuO/C_{60} core–shell nanowires were prepared by a two-step synthetic methodology involving a self-catalyzed growth of CuO nanowire core by thermally oxidizing Cu foil [22, 26] followed by a radial growth of C_{60} shell through thermal evaporation in high vacuum. CuO nanowire p-cores were grown by baking fresh copper foils (Aldrich, 99.99%) in a box oven under ambient conditions at a temperature of 500 °C for 10 h [22, 26]. C_{60} n-shells were deposited by a thermal evaporation system ($\sim 1 \times 10^{-6}$ Pa) for organic deposition [27–29]. A temperature-controlled rotated holder was used to achieve homogeneous deposition of C_{60} at a speed of 0.5 Å s^{-1}. The thickness was monitored by a quartz crystal oscillation sensor. The morphologies of core–shell CuO/C_{60} nanowires and configurations of devices based on this heterostructure were investigated by scanning electron microscopy (SEM, JSM-6700F, JEOL, Japan). The microstructures and elemental composition were examined by using a high resolution transmission electron microscope (HRTEM, JEM 2100F, JEOL, Japan) with a working voltage at 200 kV.

The core–shell CuO/C_{60} nanowires were scratched off the substrate in isopropanol alcohol (IPA) to afford a suspension. For measurements of electric transport of individual core–shell CuO/C_{60} nanowires, droplets of the suspension were spin-coated onto an Si substrate with 200 nm of thermally grown SiO_2. Lithographic patterning was used to open windows for electrodes to contact a nanowire and define a ~ 4 μm channel length. Pulsed laser deposition of 100 nm Sb-doped SnO_2 electrodes which have good light transmittance at 100 °C followed by liftoff was used to complete the two electrodes for each core–shell CuO/C_{60} nanowire. This one patterning step is used to make devices with contacts on shell–shell. For devices with contacts on core–shell, two separate patterning steps were carried out to make two electrodes, in which the C_{60} shells on CuO nanowires in the opened photoresist windows were etched for 60 min by methylbenzene before deposition of the second electrode. Last, the devices were annealed at 450 °C for 30 min in Ar to decrease the resistance of transparent Sb-doped SnO_2 electrodes and produce good contacts. The electrical and optical transport properties were measured by a Cascade probe station (Cascade Microtech, USA) connected to an Agilent E5270B 8-Slot Precision Measurement Mainframe which can reach 0.5 mV and 0.1 fA measurement resolution. The photovoltaic effects were observed under illumination of an optical illuminator (OPTEM LampLink2) connected with an optical microscopy equipped in the probe station. The average intensity was measured using a power meter at the focused position of the optical microscopy (objective lens: 20×). The spectrum of the light source shows a relative narrow emission between 400 and 700 nm with a maximum in the range of 550–600 nm.

3. Results and discussion

Figure 1(a) shows an SEM image of a single freestanding CuO nanowire with a smooth surface, of which(b) illustrates the top view of the core–shell CuO/C_{60} nanowire with the wrinkled surface of the C_{60} shell. Because of the nearly freestanding nature of as-grown CuO nanowires, isotropic and conformal shells of C_{60} were formed with approximate cylindrical geometry, as confirmed by the cross-sectional SEM image in figure 1(c). Representative TEM images of the core–shell nanowire in figure 1(d) display clearly the CuO core with a diameter of $\sim$80 nm and C_{60} shell with a thickness of $\sim$18 nm as well. The selective-area electron diffraction (SAED) result of the nanowire indicates that the growth direction of the CuO core nanowire is along [110] [22, 26]. The HRTEM image of the core–shell CuO/C_{60} nanowire in figure 1(e) reveals the single-crystalline structure of the CuO core and predominantly amorphous C_{60} shell [30, 31]. The C_{60} shell is densely and continuously packed on the interface (dashed rectangular area in figure 1(e)) with atomic scale vacancy and segregation. Theoretically, a defect-free interface is important for fast charge transfer and exciton separation.

Bright-field scanning transmission electron microscopy (STEM) in figure 2(a) reveals contrast indicative of variations in the radial chemical composition as expected from the core–shell structure. STEM energy-dispersive x-ray (EDX) mapping of the same nanowire region in figures 2(b)–(d) further confirms that the core/shell contrast observed in figures 1(d) and (e) originates from the spatial distribution of C, O and Cu

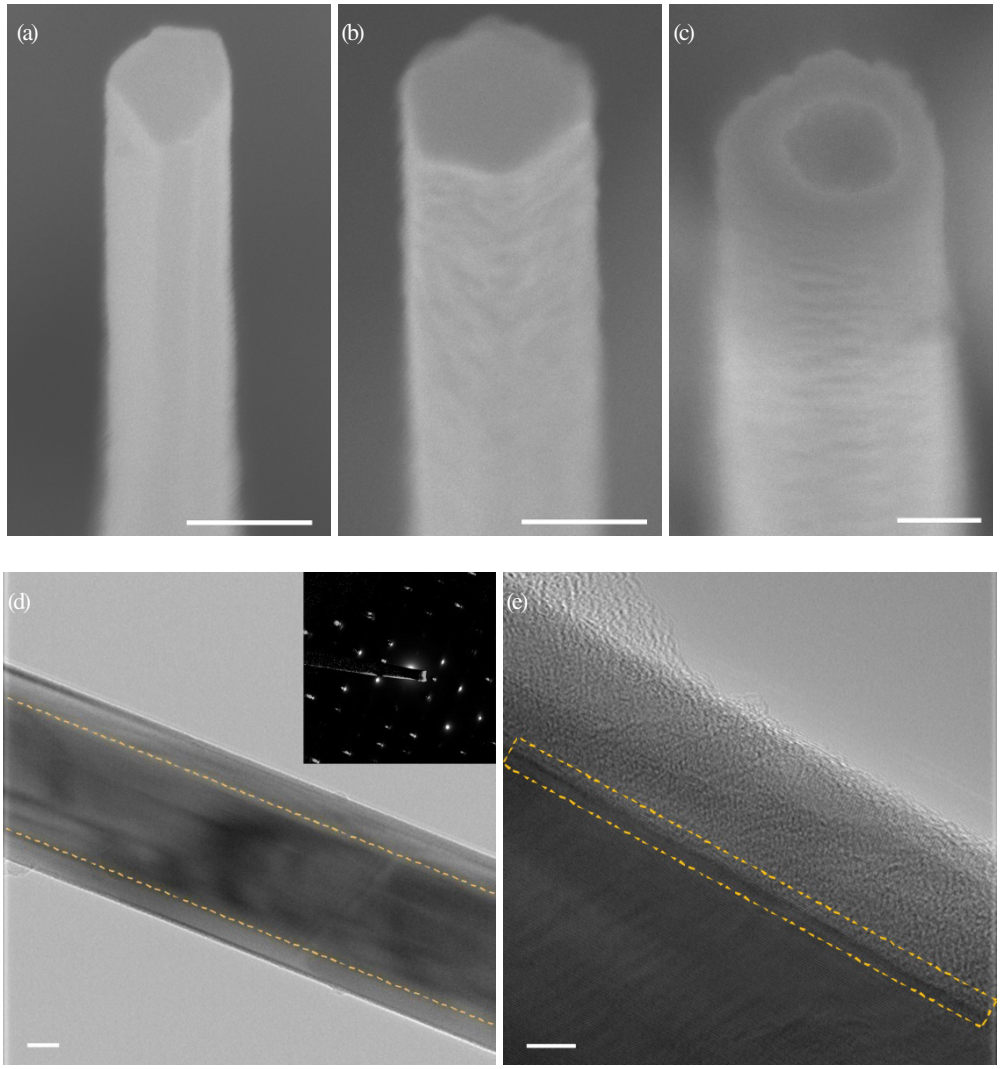

Figure 1. Electron microscopy images of CuO and core–shell CuO/C_{60} nanowires. (a) SEM image of CuO nanowire from top view. (b) SEM image of CuO nanowire coated with C_{60} from top view. (c) SEM image of cross section of core–shell CuO/C_{60} nanowire. The scale bars in (a)–(c) are all 100 nm. (d) TEM image of core–shell CuO/C_{60} nanowire (scale bar is 20 nm), the inset shows SAED from this core–shell nanowire. (e) HRTEM image of core–shell CuO/C_{60} nanowire (scale bar is 5 nm). The dashed yellow lines in (d), (e) highlight the interface between CuO and C_{60}.

elements in the shell and core, respectively. Even though the elemental mapping of C does not clearly show a sharp interface between CuO and C_{60}, a quantitative analysis reveals that the diameter of the CuO core is ∼135 nm and the thickness of the C_{60} shell is ∼20 nm, which is in agreement with the targeted core–shell heterostructure. The STEM elemental line scan in figure 2(e) across the CuO/C_{60} nanowire in figure 2(a) further demonstrates the core–shell structure. It can be observed that the nanowire 'core–shell' structure in figure 2 is not absolutely coaxial and its one side has higher carbon (figure 2(e)), thus not showing a sharp interface between CuO and C_{60}. However, the experimental results discussed above clearly confirm the core–shell structure.

The electric transport properties of the core–shell CuO/C_{60} nanowire heterostructure were studied in a two-probe configuration with transparent SnO_2 anode [32]. Three types of devices with contacts on core–core, core–shell and shell–shell were fabricated. Figure 3(a) illustrates a schematic of the devices with the core–shell and shell–shell contacts. Dark current–voltage (I–V) curves obtained from these devices are shown in figure 3(b) and demonstrate several notable features. The linear I–V curve from the core–core (CuO–CuO) configuration indicates ohmic contacts made on the CuO nanowire. The I–V curve for the shell–shell contact exhibits a Schottky barrier existing between the C_{60} shell and SnO_2 electrodes, and the shell conductance of C_{60} is much smaller than that of the CuO core. Furthermore, the I–V curve obtained from the core–shell contact shows rectifying behavior and demonstrates that the p–n coaxial CuO/C_{60} nanowires behave as well-defined diodes. For this coaxial CuO/C_{60} nanowire p–n junction, current is blocked when it is biased negatively (*reverse* bias), but when the polarity is switched to the opposite the current starts to increase until a voltage threshold of 0.2 V, beyond which the current does not increase under the positive bias, indicating a built-in electrical field at the interface p-CuO/n-C_{60}. Responses to illumination

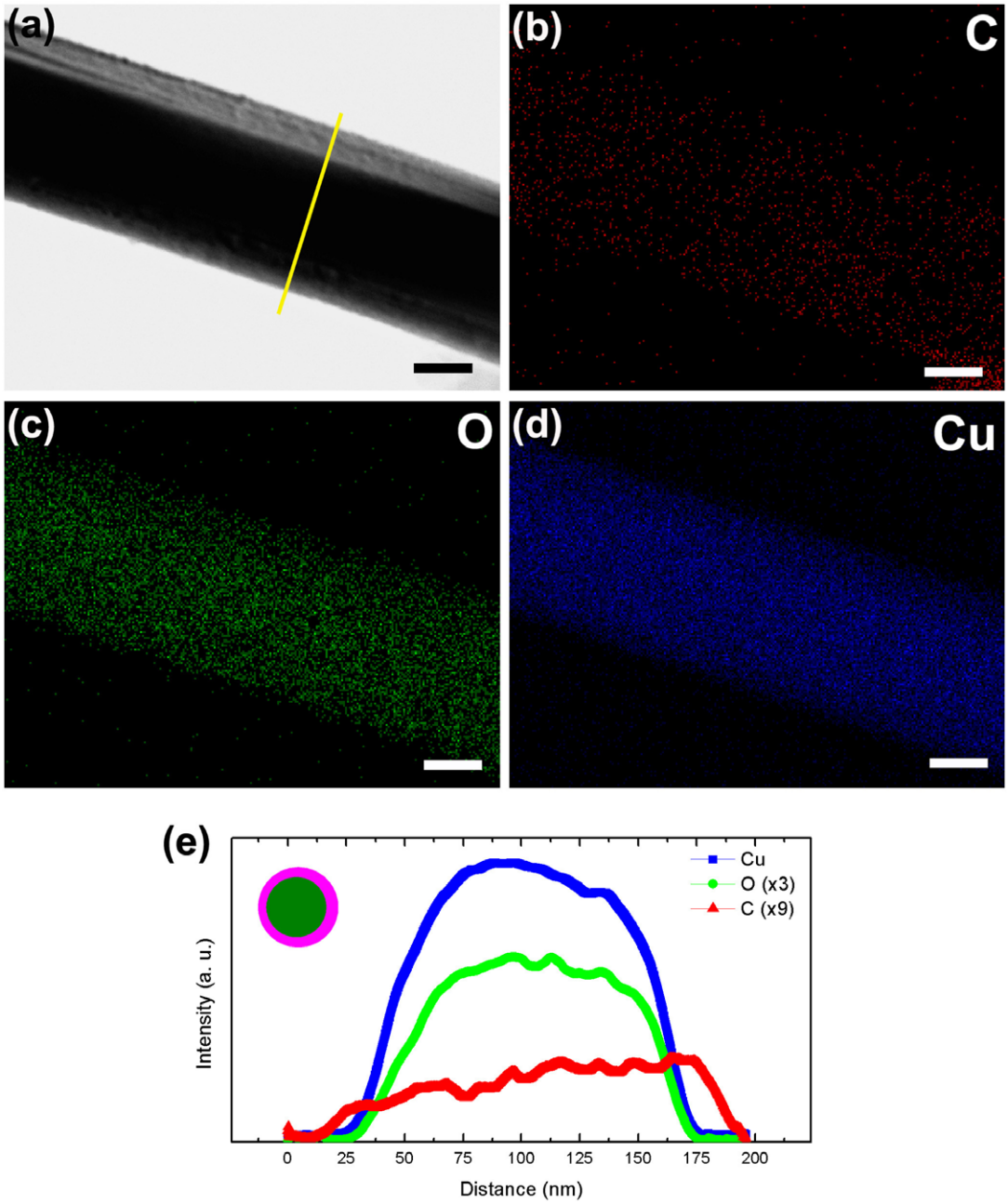

Figure 2. STEM elemental mapping and line scan of core–shell CuO/C_{60} nanowire. (a) Bright-field image of a core–shell CuO/C_{60} nanowire. (b)–(d) STEM elemental maps of C (red) O (green) and Cu (blue) concentrations, respectively, in the nanowire of (a). The scale bars in (a)–(d) are all 50 nm. (e) STEM elemental line scan across the core–shell CuO/C_{60} nanowire in (a). The inset shows a schematic cross section of the core–shell structure.

of the CuO/C_{60} nanowire heterostructure are then expected accordingly.

Figure 3(c) shows a semi-log scale plot of the *forward* bias dark I–V data from the CuO/C_{60} nanowire heterostructure with core–shell contacts, from which the ideality factors, n, ranging from 2.0 to 10.0, can be extrapolated. Typically, the devices showed that the ideality factor for biases from 0.15 to 0.3 V, from 0.4 to 1.2 V, and higher than 1.2 V was ∼2.34, ∼5.98 and ∼9.87, respectively. The ideality factors at lower bias are comparable to the ideality factors reported for inorganic/C_{60} heterojunctions [6, 7]. The series resistance observed at high *forward* biases (>1.2 V) was approximately equal to the wire resistance plus the contact resistance. Reverse breakdown occurred beyond −2 V (figure 3(a)), a value very near the expected threshold for avalanche or tunnel breakdown [33].

To analyze the transport mechanism inside the CuO/C_{60} nanowire heterostructure, I–V and logarithmic I–V curves at various temperatures were recorded, as shown in figure 4. In general, for the thin-film semiconductor heterojunctions two possible models, the thermionic and the tunneling, are often responsible for the transport mechanism [34–36]. Their

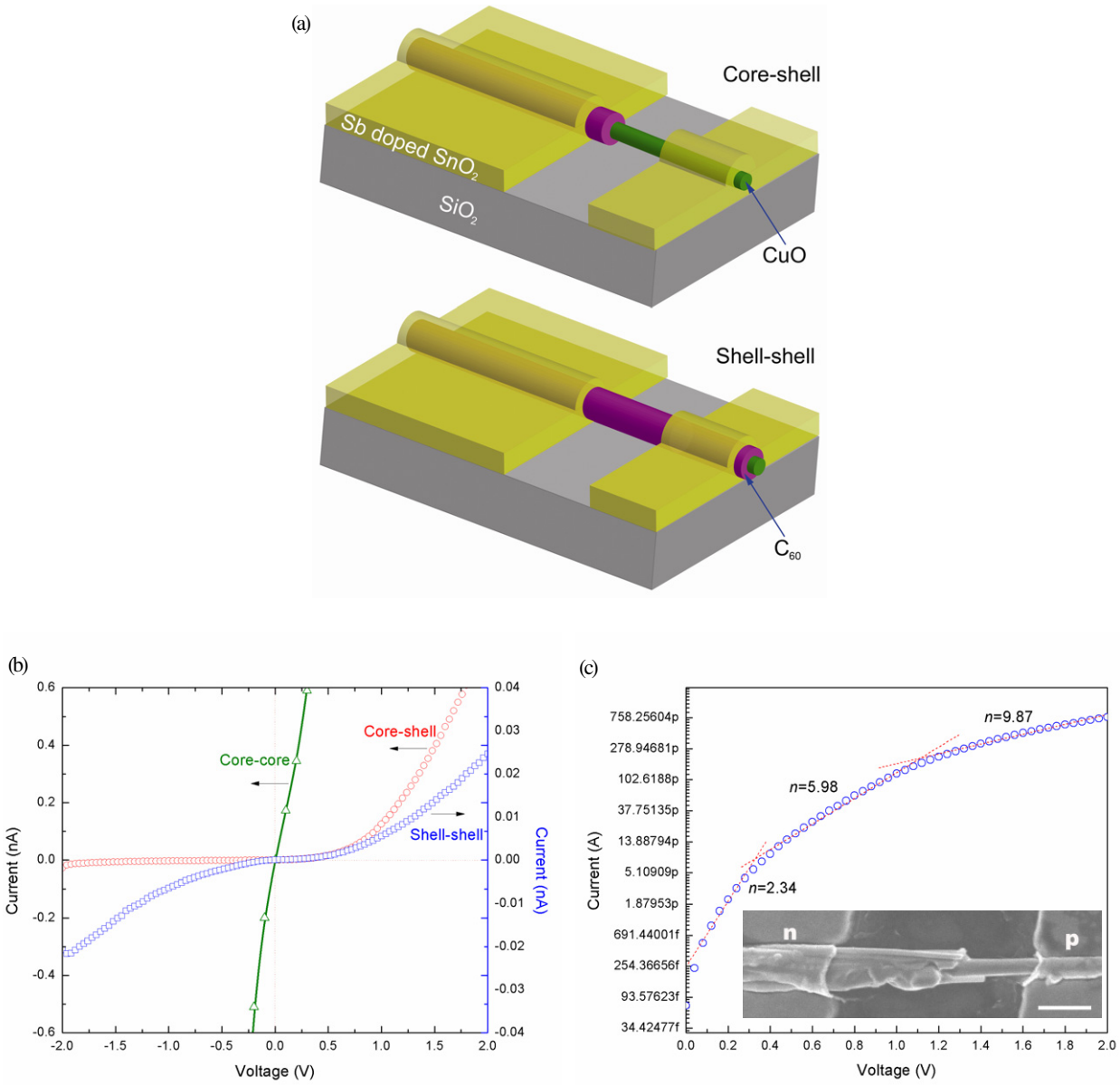

Figure 3. (a) Schematics of devices with contacts on core–shell (up) and shell–shell (down). (b) Typical dark I–V curves of three types of devices with contacts on core–core, core–shell and shell–shell. (c) Semi-log scale plot of the forward bias dark I–V data of device with contacts on core–shell. The linear fits illustrate the extracted diode ideality factor, n. The inset is an SEM image of the device which clearly shows the p–n junction formed by core–shell contact (scale bar: 1 μm).

mathematical formulations are

$$\log(I) = \log(I_0) + qV/kT \tag{1}$$

$$\log(I) = \log(I_0) + aV \tag{2}$$

where k is the Boltzmann constant, q is the electron charge, I_0 is the saturation current extrapolated from the logarithmic I–V curve and α is a constant related to the tunneling barrier of the junction. The determinant difference between the two transport mechanisms is the temperature dependence of the slope of the $\log(I)$–V curve. The slope is temperature-dependent in the thermionic model but is insensitive to temperature in the tunneling model. It is found that the slope of the curves (shown by yellow lines) in both panels (b) and (d) of figure 4 are not sensitive to the temperature, which indicates that the transport of the CuO/C_{60} heterojunction could be ascribed to the tunneling model. Furthermore, the reverse bias breakdown voltage of the CuO/C_{60} p–n diode increases with decreasing temperature, which is consistent with a Zener (tunneling) breakdown mechanism [19].

The core–shell CuO/C_{60} nanowire heterostructure was further electrically characterized with illumination and a photovoltaic effect was observed. The devices with contacts on core–shell have responses to the optic illuminator with a short-circuit current I_{sc}, which are not observed from devices with two contacts on shell (C_{60}) or core (CuO). Switch on/off of the illuminator causes the generation/annihilation of I_{sc} alternatively, as shown in figure 5(a). The I–V curves with

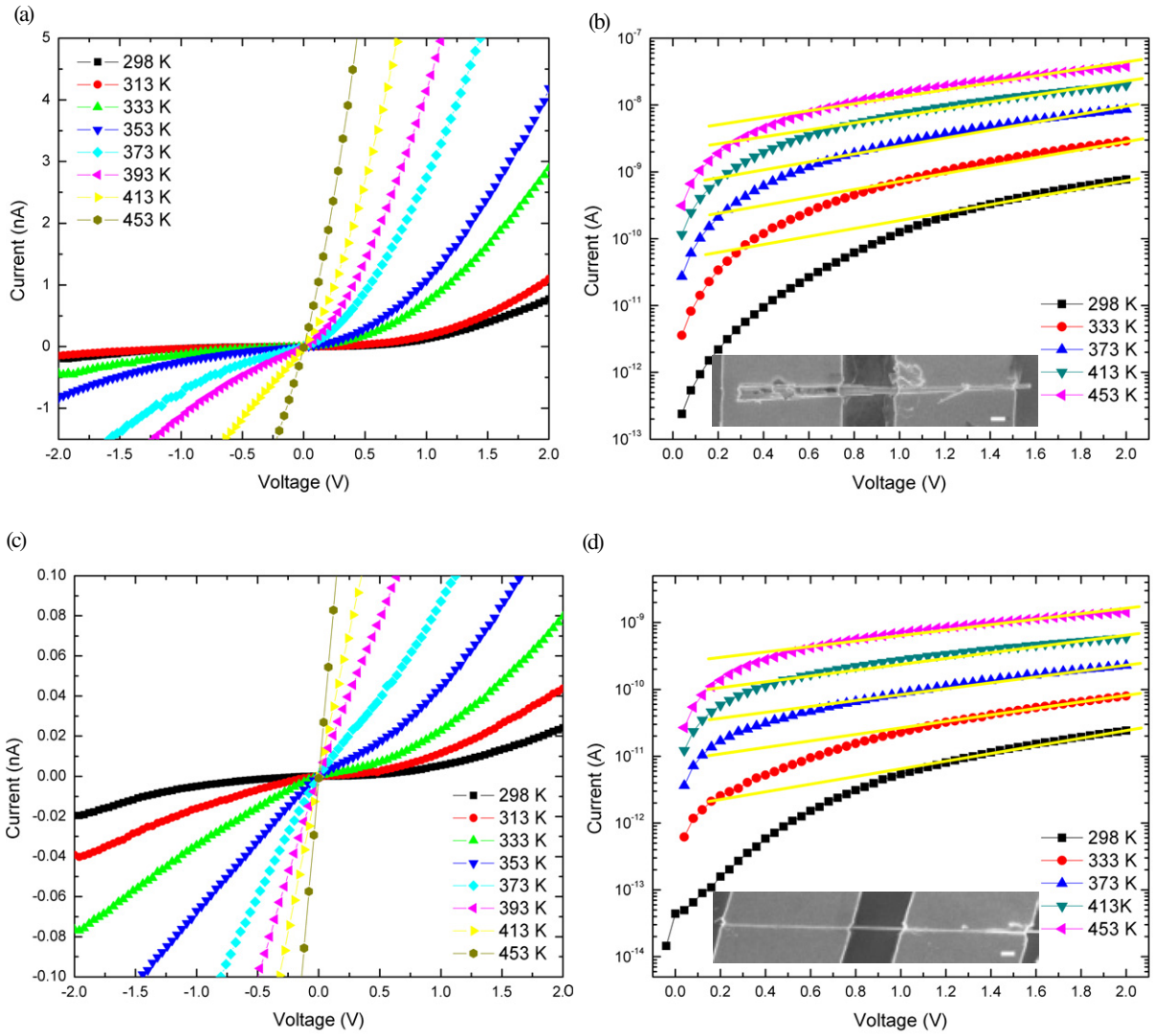

Figure 4. (a) I–V and (b) logarithmic I–V curves of CuO/C_{60} nanowire with core–shell contacts at different temperatures. Inset in (b) shows the SEM image of the measured device (scale bar: 1 μm). (c) I–V and (d) logarithmic I–V curves of CuO/C_{60} nanowire with shell–shell contacts at different temperatures. Inset in (d) shows the SEM image of the measured device (scale bar: 1 μm).

and without illuminations are compared in figure 5(b), from which a filling factor, f of 0.26 is obtained. The short-circuit current density J_{sc} of 0.28 mA cm^{-2} is estimated via a methodology of using the projected area, which is commonly applied to the nanowire photovoltaic devices [19, 37, 38]. The maximum power output P_{max} for the core–shell CuO/C_{60} nanowire device is 70 fW. The photovoltaic efficiency of the core–shell CuO/C_{60} p–n heterostructure is then calculated by the conversion equation:

$$\eta = f J_{sc} V_{oc} / P_{input} \tag{3}$$

where η is the efficiency, f is the filling factor and P_{input} is the input power density. The photovoltaic efficiency of the measured devices was estimated to be less than 0.02% considering the errors of the measured input power density. The overall apparent efficiency of the core–shell CuO/C_{60} p–n heterostructure could be increased substantially with improvements in V_{oc} by improving the crystalline structure of the shells and/or passivating the nanowire surface [19, 20].

The inset of figure 5(b) illustrates the schematic energy diagram for the CuO/C_{60} nanowire heterojunction based on vacuum levels of CuO and C_{60}. The Fermi level of C_{60} is closer to the lowest unoccupied molecular orbital (LUMO)-derived band than the highest occupied molecular orbital (HOMO)-derived band [5]. The energy level of CuO with conduction band E_c = 4.07 eV and valence band E_v = 5.42 eV [21, 22, 39] aligns very well with LUMO- and HOMO-derived bands of C_{60} (4.2 eV and 5.7–6.0 eV) [40, 41]. The effective barrier height shown in the diagram (inset of figure 5(b)) can be increased and reduced under reverse and forward biases, respectively, resulting in strong rectification of the CuO/C_{60} heterojunction. The built-in electrical field at the interface of CuO/C_{60} and the inherent high electron affinity of C_{60} molecules drives the electron transfer from CuO to C_{60} under illumination. The work function of the transparent

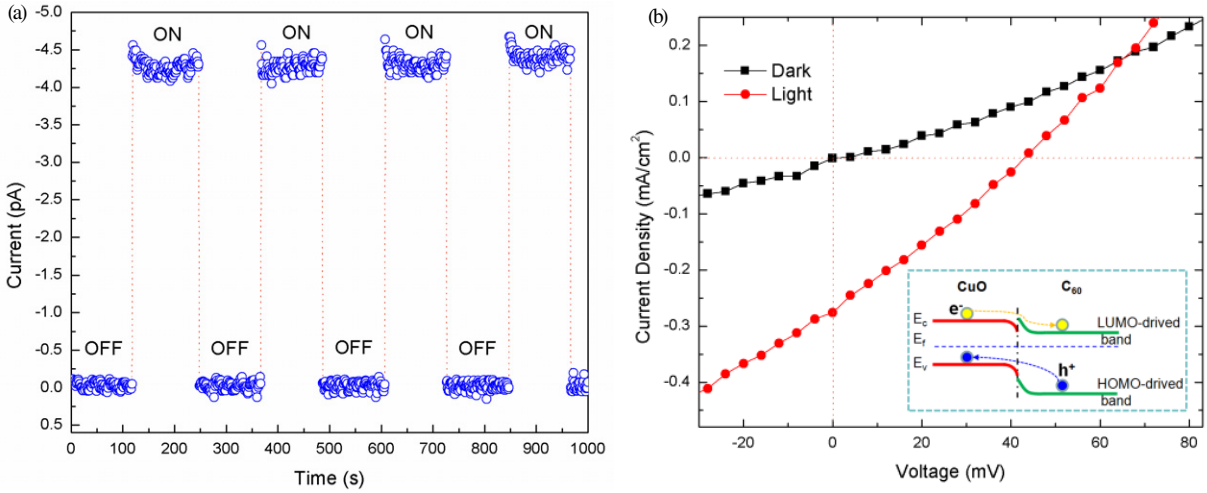

Figure 5. Photovoltaic effects of core–shell CuO/C_{60} nanowire devices with contacts on core–shell. (a) Real-time record of the I_{sc} of a CuO/C_{60} nanowire device illuminated by an optic illuminator. (b) Dark/light J–V data with current density normalized to the light absorption cross-sectional area. The inset is the schematic energy level diagram for CuO and C_{60} showing the possible charge transfer.

electrodes, Sb-doped SnO_2, is about 4.7–5.7 eV [42–44], which is comparable to those of CuO nanowires (5.2 eV) [39] and C_{60} (4.7 eV) [5] and can make the charge carriers easily leading out.

It is worth noting that the presence of dipoles at most semiconductor interfaces during charge transfer may result in a dipole potential and building electrical field, which could cause modification of the band alignment. It will be good to use photoelectron spectroscopy to study the band alignment at the CuO/C_{60} interface in future work. Furthermore, some other factors might also contribute to the observed electrical and optical transport phenomenon: the adoption of the semiclassical model should be considered as a qualitative approach rather than a complete interpretation of the tunneling transport behavior and photovoltaic effects of such organic/inorganic p–n heterojunctions.

4. Conclusions

In summary, we have designed and synthesized a core–shell CuO/C_{60} nanowire heterojunction which, revealed by TEM studies, has a single-crystal CuO core with a ∼20 nm amorphous C_{60} shell, and is further confirmed by energy-dispersive x-ray spectroscopy analysis for the heterostructure. Systematic electrical transport studies confirm the coaxial nanowire p–n junction and demonstrated the tunneling transport mechanism. Photovoltaic effects of the devices were observed with contacts on core–shell when the devices were illuminated. In this work, most of the CuO nanowires are in the range of 50–100 nm. The device performance could be further improved by fabrication of nanowires down to ∼20 nm range, leading to less charge recombination for higher exciton dissociation. These devices can be used to gain insight into the performance-determining properties for nanowire photovoltaics, such as the resistivity, diffusion length and rates of bulk and surface recombination in one-dimensional nanostructures. This work lays the groundwork for further studies on organic–inorganic hybrid nanowire devices and enables a new concept of photovoltaic devices by packing core–shell nanowires densely both in the substrate plane and in a three-dimensional stack for renewable energy technologies.

Acknowledgments

This work was financially supported by Singapore A*STAR grant no. 052 117 0031. One of the authors (LL) acknowledges support in this work by the Singapore Millennium Foundation 2008 scholarship.

References

[1] Gratzel M 2001 *Nature* **414** 338–44
[2] Law M, Greene L E, Johnson J C, Saykally R and Yang P D 2005 *Nat. Mater.* **4** 455–9
[3] Coronado E and Palomares E 2005 *J. Mater. Chem.* **15** 3593–7
[4] Khan A, Yamaguchi M and Kojima N 2000 *Solid-State Electron.* **44** 1471–5
[5] Kita K, Wen C, Ihara M and Yamada K 1996 *J. Appl. Phys.* **79** 2798–800
[6] Chen K M, Sun W H, Wu K, Li C Y, Qin G G, Zhang Q L, Zhou X H and Gu Z N 1999 *J. Appl. Phys.* **85** 6935–7
[7] Sun W H, Chen K M, Wu K, Li C Y, Zhang Q L, Zhou X H, Gu Z N and Qin G G 2000 *Solid-State Electron.* **44** 555–8
[8] Huynh W U, Dittmer J J and Alivisatos A P 2002 *Science* **295** 2425–7
[9] Huynh W U, Dittmer J J, Teclemariam N, Milliron D J, Alivisatos A P and Barnham K W J 2003 *Phys. Rev.* B **67** 115326
[10] Gur I, Fromer N A, Chen C P, Kanaras A G and Alivisatos A P 2007 *Nano Lett.* **7** 409–14
[11] Liu J, Tanaka T, Sivula K, Alivisatos A P and Frechet J M J 2004 *J. Am. Chem. Soc.* **126** 6550–1
[12] Beek W J E, Wienk M M and Janssen R A J 2006 *Adv. Funct. Mater.* **16** 1112–6
[13] Beek W J E, Wienk M M and Janssen R A J 2004 *Adv. Mater.* **16** 1009–13
[14] Beek W J E, Wienk M M, Kemerink M, Yang X and Janssen R A J 2005 *J. Phys. Chem.* B **109** 9505

[15] McDonald S A, Konstantatos G, Zhang S G, Cyr P W, Klem E J D, Levina L and Sargent E H 2005 *Nat. Mater.* **4** 138–42
[16] Gunes S, Neugebauer H, Sariciftci N S, Roither H, Kovalenko M, Pillwein G and Heiss W 2006 *Adv. Funct. Mater.* **16** 1095–9
[17] Zhang Y, Wang L W and Mascarenhas A 2007 *Nano Lett.* **7** 1264–9
[18] Kayes B M, Atwater H A and Lewis N S 2005 *J. Appl. Phys.* **97** 114302
[19] Tian B Z, Zheng X L, Kempa T J, Fang Y, Yu N F, Yu G H, Huang J L and Lieber C M 2007 *Nature* **449** 885–90
[20] Garnett E C and Yang P 2008 *J. Am. Chem. Soc.* **130** 9224–5
[21] Gou X L, Wang G X, Yang J S, Park J and Wexler D 2008 *J. Mater. Chem.* **18** 965–9
[22] Liu Y L, Liao L, Li J C and Pan C X 2007 *J. Phys. Chem.* C **111** 5050–6
[23] Hoppe H and Sariciftci N S 2004 *J. Mater. Res.* **19** 1924–45
[24] Sariciftci N S, Braun D, Zhang C, Srdanov V I, Heeger A J, Stucky G and Wudl F 1993 *Appl. Phys. Lett.* **62** 585–7
[25] Lof R W, Vanveenendaal M A, Koopmans B, Jonkman H T and Sawatzky G A 1992 *Phys. Rev. Lett.* **68** 3924–7
[26] Yu T, Zhao X, Shen Z X, Wu Y H and Su W H 2004 *J. Cryst. Growth* **268** 590–5
[27] Song Q L, Li C M, Chan-Park M B, Lu M, Yang H and Hou X Y 2007 *Phys. Rev. Lett.* **98** 176403
[28] Song Q L, Li C M, Wang M L, Sun X Y and Hou X Y 2007 *Appl. Phys. Lett.* **90** 071109
[29] Song Q L, Wang M L, Obbard E G, Sun X Y, Ding X M, Hou X Y and Li C M 2006 *Appl. Phys. Lett.* **89** 251118
[30] Dravid V P, Liu S Z and Kappes M M 1991 *Chem. Phys. Lett.* **185** 75–81
[31] Jin Y Z, Curry R J, Sloan J, Hatton R A, Chong L C, Blanchard N, Stolojan V, Kroto H W and Silva S R P 2006 *J. Mater. Chem.* **16** 3715–20
[32] Yang F and Forrest S R 2006 *Adv. Mater.* **18** 2018–22
[33] Sze S M and Kwok K N 2007 *Physics of Semiconductor Devices* (Hoboken, NJ: Wiley)
[34] Riben A R and Feucht D L 1966 *Solid-State Electron.* **9** 1055–65
[35] Zeidenbergs G and Anderson R L 1967 *Solid-State Electron.* **10** 113–23
[36] Anderson R L 1962 *Solid-State Electron.* **5** 341–4
[37] Kelzenberg M D, Turner-Evans D B, Kayes B M, Filler M A, Putnam M C, Lewis N S and Atwater H A 2008 *Nano Lett.* **8** 710–4
[38] Liang C-W and Roth S 2008 *Nano Lett.* **8** 1809–12
[39] Koffyberg F P and Benko F A 1982 *J. Appl. Phys.* **53** 1173–7
[40] Chase S J, Bacsa W S, Mitch M G, Pilione L J and Lannin J S 1992 *Phys. Rev.* B **46** 7873
[41] Tsuei K-D, Yuh J-Y, Tzeng C-T, Chu R-Y, Chung S-C and Tsang K-L 1997 *Phys. Rev.* B **56** 15412
[42] Bhise A B, Late D J, Walke P S, More M A, Pillai V K, Mulla I S and Joag D S 2007 *J. Cryst. Growth* **307** 87–91
[43] Wan Q, Dattoli E N and Lu W 2007 *Appl. Phys. Lett.* **90** 222107
[44] Batzill M and Diebold U 2005 *Prog. Surf. Sci.* **79** 47–154